Eidgenössische Technische Hochschule Zürich
Swiss Federal Institute of Technology Zurich

Institute for Particle Physics

Experimental semester project

Temperature and Irradiation Effects on the Threshold of the digital Readout Chip for the Phase I Upgrade of the CMS Pixel Detector

Author:
Daniele Ruini

Group leader:
Prof. Dr. Rainer Wallny

Head of laboratory:
Dr. Andrey Starodumov

Supervisor:
Jan Hoss

July 14, 2015

Abstract

The Phase I Upgrade of the CMS pixel detector, planned for 2016, foresees, among other changes, the substitution of the current analog readout chips. In layers two to four of the new detector the digital chip *psi46V2.1respin* will be used. This work analyses the threshold of the new chip for temperature and irradiation dose dependent effects. After reproducibility tests of the threshold parameters at constant conditions, temperature studies show that with a fixed parameter configuration the threshold increases linearly with temperature with a slope of 0.2 *Vcal* DAC units/K. This shift can be corrected for by adjusting the *VthrComp* DAC according to a linear parametrization with a slope of 0.2 DAC units/K. All other parameters show no temperature dependence. As a tradeoff for the correction, the width of the trimmed threshold distribution slightly increases from 51 electrons to 64 electrons. Irradiation causes for most samples a shift of the trim bits to higher values, which results in a dose dependent shift of the threshold to lower *Vcal* values and an increase of the width of the trimmed threshold distribution by a factor 2-3. The shift can be compensated for by a correction of the *VthrComp* DAC, while no viable solution has been found to obtain a narrow threshold distribution after irradiation at the detector; for technical reasons a re-optimization of all threshold parameters at CMS is currently not an option.

Contents

1. Introduction

Particle accelerators are the most important tool for research in modern high energy physics. From 1909 on, when Rutherford preformed his famous gold foil experiment [Rut11], larger and larger machines have been built to accelerate particles to higher and higher energies so as to investigate nature at smaller and smaller scales. This chapter briefly introduces the world's largest and most powerful accelerator, the Large Hadron Collider (LHC), and one of its experiments, the Compact Muon Solenoid (CMS) detector.

1.1 The Large Hadron Collider

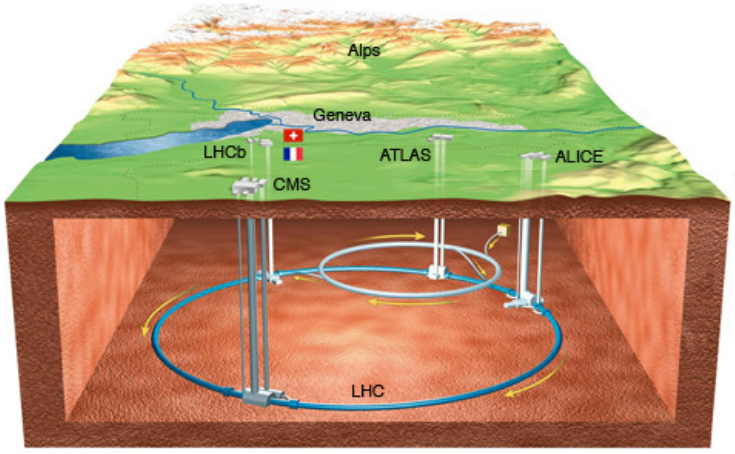

Figure 1.1: A sketch of the LHC ring and the experiments [CER15a].

The LHC is located at CERN, Geneva, in a 27 km long circular tunnel about 100 m underground. As its name indicates, it is designed to accelerate hadrons, i.e. particles made of quarks. These particles are usually protons, but also lead ions can be accelerated. Particles travelling at nearly the speed of light circulate in opposite directions in two separate beam pipes and collide in four interaction points where the detectors are located. The acceleration is reached through eight superconducting cavities per beam,

while the bending on circular trajectories and the focusing of the beams is achieved by superconducting dipole and quadrupole magnets. The first data sets were recorded in 2010 at a centre of mass energy of 7 TeV. After a development phase during 2013/14, called Long Shutdown 1 (LS1), the energy was increased and in June 2015 the first proton-proton collisions at 13 TeV were recorded [CER15b]. Together with the beam energy also the luminosity, i.e. the number of collisions per second and unit beam cross section, is planned to increase from a peak value of about $7 \times 10^{33}\,\mathrm{cm}^{-2}\,\mathrm{s}^{-1}$ in 2012 [LHC12] to up to $2 \times 10^{34}\,\mathrm{cm}^{-2}\,\mathrm{s}^{-1}$ in the coming years. This means that more data can be recorded, but also sets harsher conditions in which the detectors have to be operated. To meet the more demanding requirements, several upgrades are necessary. This project is related to one of these upgrades - the replacement of the pixel detector of the CMS experiment, which is introduced in the next section.

1.2 The Compact Muon Solenoid detector

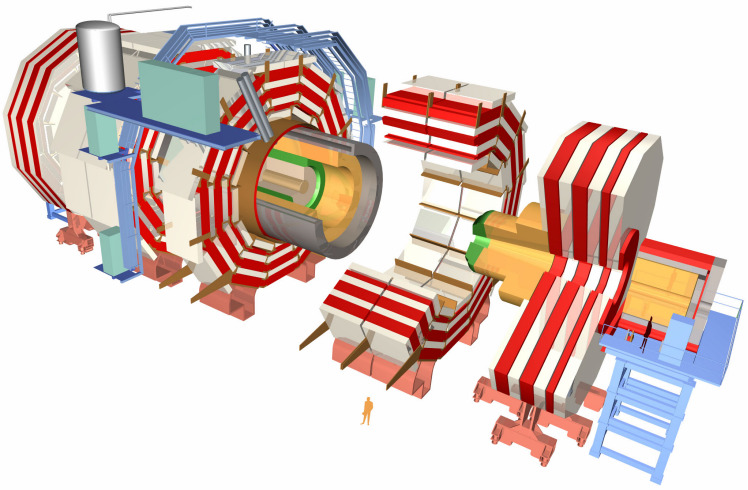

Figure 1.2: The CMS detector has a cylindrical structure around the beam axis closed by two end caps to provide the best angular coverage. Both the barrel section and the end caps consist of different subdetectors arranged in a multilayered structure, each of which serves a specific purpose [DES15].

CMS is one of the two general purpose detectors at the LHC. Its main goals are to study the Higgs boson, which has been discovered in 2012 [ATL12, CMS12], to look for new physics beyond the Standard Model and to measure known phenomena with higher precision. To do this, the detector must be able to detect and identify the particles that are created during collisions and measure their properties like position, energy and momentum with the

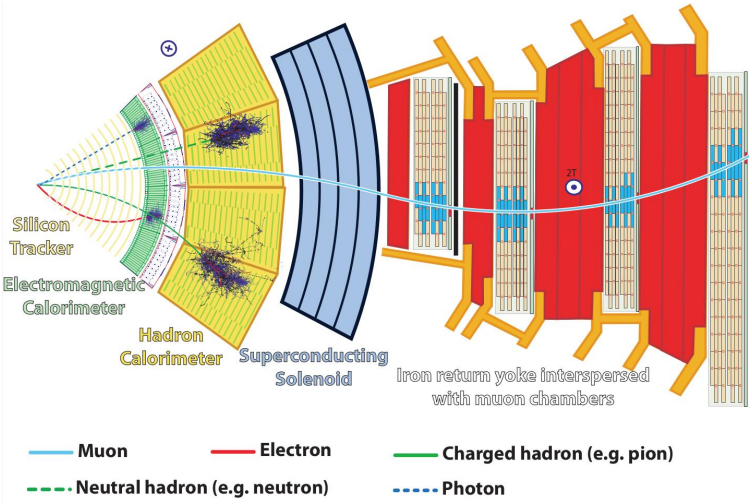

Figure 1.3: Cut view of the barrel section of the CMS detector. From left to right there are the interaction point and the different subdetectors described in the main text. Also shown are the signatures of some of the particles generated in the collisions [CMS15].

best possible resolution and geometrical coverage. It is therefore arranged in a barrel structure with two end caps around the beam axis as shown in Figure 1.2 and consists of several subdetectors, each one of which serves a different purpose. Figure 1.3 shows the different components of the detector in a transverse slice of the barrel section and the signatures of different types of particles. From inside out the different subdetectors are:

Silicon tracker, to measure the trajectories of charged particles. Close to the interaction point, where the particle flux is highest, it consists of a pixel detector, while at greater radii a silicon strip detector is used. Being the central component of this project, the pixel detector will be described in detail in Chapter 2.

Calorimeters, to measure the energy of the particles. This is done by absorbing the particles with blocks of matter and by measuring the deposited energy with scintillators. Because of the different properties of the produced particles two types of calorimeter are needed: the inner one absorbs electrons and photons and is called electromagnetic calorimeter, the outer one, called hadronic calorimeter, measures the energy of hadrons.

Superconducting solenoid to generate the magnetic field in the direction along the beam axis that bends the trajectories of charged particles. The bending radius, measured with the tracking device, allows to reconstruct the momentum of charged particles. The magnetic field also

filters out uninteresting low momentum particles, since for them the radius is so small that they move in tight spirals and never reach the tracker. A so called return yoke is placed outside the solenoid to guide the magnetic field in this region.

Muon chambers interspersed with the return yoke to detect muons, since these particles are the only ones to pass through all layers of the detector, because of their high mass and insensitivity to the strong interaction.

The amount of data produced is by far too large to be stored entirely. Therefore the detector is completed by a complex trigger and data acquisition system, which decides which events are interesting and should be saved and which only contain well known physics and can be discarded.

2. Pixel detector

The pixel detector is the inner part of the tracking device and the component of CMS closest to the beam pipe. Its purpose is to track the trajectories of charged particles as close as possible to the interaction point. To this end, it has to satisfy the following requirements:

High spatial resolution for precise vertex reconstruction.

Radiation hardness to avoid performance losses due to exposure to high particle fluxes.

Low material budget to avoid multiple scattering and unnecessary energy absorption; the energy lost in the tracker cannot be measured by the calorimeters any more.

Fast readout because of the high collision frequency and the high track density due to multiple collisions in one bunch crossing (pile-up) which produce very high occupancies.

After briefly summarizing the basic properties of semiconductors, this chapter describes the structure and working principle of the CMS pixel detector.

2.1 Basic physics of semiconductors

The basic principle of the tracking detector is that a charged particle that crosses it should induce an electrical charge which can be measured. This can be implemented with semiconducting materials arranged in a so called pn-junction.

Semiconductors. Materials like silicon have a small energy gap between the valence and the conduction band which can be easily overcome by thermally or ionization induced excitations. This means that the concentration of free charge carriers (and thus the conductivity) is strongly temperature dependent. The excitations induced by radiation are the principle on which semiconductor detectors work. This effect is however by orders of magnitude smaller than thermal excitations. Charge carriers freed by a passing

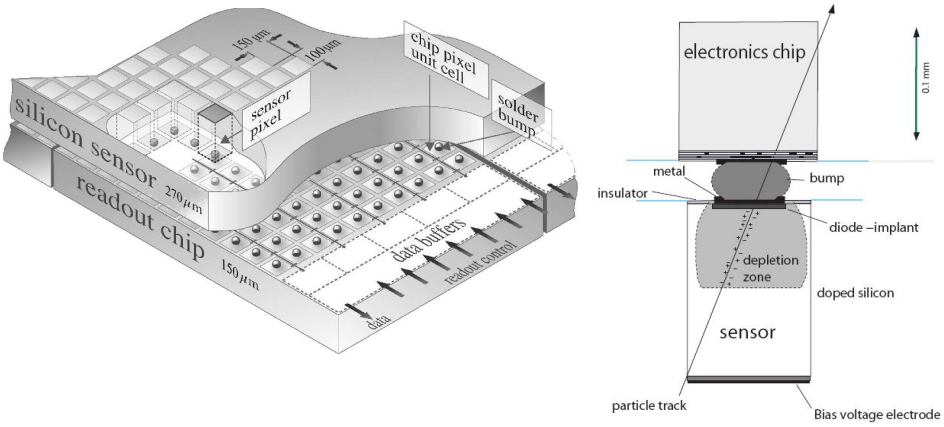

(a) *(b)*

Figure 2.1:

(a) Cutaway sketch of the sensor divided in pixels and the underlying readout chip [C+09].

(b) Cut view of a single pixel. At the bottom there is the Si sensor with applied bias voltage, bump bonded to the electronics of the readout chip at the top [R+06].

particle are thus undetectable above the background of the intrinsic ones at any reasonable working temperature of the detector. This problem is solved by bringing two layers of differently doped materials close together in a pn-junction.

Doping. P-type silicon (Si) contains a small amount of atoms from the third main group of the periodic table, e.g. boron, resulting in a lack of electrons and thus in an additional acceptor layer just above the valence band; n-type Si contains instead impurities from the fifth group, e.g. phosphorus, which create an additional donor level slightly below the conduction band. When two layers of p- and n-type Si are brought together, the excess electrons from the n-doped side drift through the boundary surface to fill the acceptor level of the p-doped Si and thus induce an electric field. The drift stops once the electric field exceeds a certain threshold. This effect removes the free charge carriers from the region around the boundary surface, which is then called depletion zone. The depletion zone can be extended by applying a so called reverse bias, i.e. a voltage with the same polarity as the drift induced field. In this way the concentration of intrinsic charge carriers can be effectively reduced, allowing to detect a radiation induced signal.

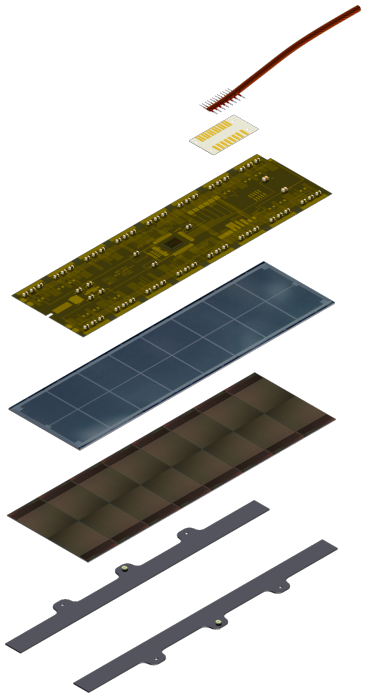

Figure 2.2: Exploded view of a pixel detector module; from top to bottom it consists of a shared cable for power and signal, the token bit manager, the high density interconnect, the silicon sensor, the ROCs and base strips to provide mechanical stability [D⁺12].

2.2 Structure of the detector

The properties of semiconductors discussed in the previous section are exploited to build sensors that are able to detect charged particles produced during collisions at CMS. The sensor consists of a highly resistive n-substrate in which highly doped n++ implants, called pixels, are embedded. A p-substrate on the backplane forms the pn-junction. Pixels measure (150×100) μm^2 and each one of them is read out individually to get hit information. The pixel structure, shown in Figure 2.1(a), provides a two dimensional spatial resolution. Figure 2.1(b) shows the structure of a single pixel. When a charged particle traverses the sensor, it creates free electron-hole pairs which are collected at the electrodes by the applied voltage. This charge is then read out by the electronics of the so called pixel unit cell (PUC), to which the Si sensor is connected through a metallic bump bond. The matrix of PUCs together with control and interface electronics and the data and timestamp buffers form the readout chip (ROC) which is described in detail in the next section. ROCs are assembled into an 8×2 array to form a module, an exploded view of which is shown in Figure 2.2. From top to bottom it consists of: a shared cable for power and signal, the token bit manager (TBM) which organizes the data readout, the high density interconnect (HDI) which distributes the power as well as signal, trigger and clock information, the silicon sensor, the ROCs and base strips to provide mechanical stability. To obtain three dimensional resolution of the particle trajectories, modules are arranged in different layers on top of each other. Fitting the points hit in each layer allows then to reconstruct the trajectory of the particle.

2.3 The readout chip

This section describes the digital ROC *psi46V2.1respin*. ROCs are, together with the silicon sensors, the central component of the CMS pixel detector. Each ROC consists of 80 rows and 52 columns of pixels, organized in 26 double columns; each one of these is linked to a double column interface (DCI), which reads out and stores the signal. The readout from different DCIs is controlled by the control and interface block (CIB). A scheme of the readout chain of a ROC is shown in Figure 2.3. The bump pad in the top left of the picture connects the PUC to the silicon sensor. The signal generated in the sensor by a particle is first amplified and shaped; then, if it exceeds a certain threshold, it is stored in the DCI. The data from all DCIs is collected in a readout buffer while waiting for trigger verification and, if the decision is positive, sent to the periphery.

The configuration of a ROC is controlled via 16 digital to analog converters (DACs). Not all DACs are relevant for this project, and only those that are will be described in the following. The analog current of the ROC is adjusted via the *Vana* DAC. For testing purposes a signal can be faked by injecting a calibration pulse; the strength of this signal can be set through the *Vcal* DAC. One *Vcal* DAC unit corresponds to approximately 46 electrons. The calibration pulses can be delayed by setting a DAC called *CalDel*. Other relevant parameters are those that regulate the threshold to which the signal is compared. The global threshold of the ROC can be adjusted with the *VthrComp* DAC; low values of this parameter correspond to high thresholds and high values to low thresholds. Note that this is not enough to obtain a uniform threshold distribution, since the performance of shaper, amplifier and comparator slightly varies among pixels. To obtain a uniform threshold for all pixels, each PUC is provided with four trim bits to individually adjust its threshold. The strength of the trim bits, i.e. how much each trim bit step influences the threshold, is regulated with the *Vtrim* DAC (this is again a global DAC for the whole ROC). Note that *VthrComp* and *Vtrim* are 8 bit DACs, which means that they can take values between 0 and 255, while the four trim bits can take values between 0 and 15.

2.4 Phase I Upgrade of the CMS pixel detector

As mentioned above, after LS1 the detector will be exposed to tighter conditions of increased centre of mass energy and luminosity. Moreover, the performance of the current detector will eventually degrade due to radiation damage. A complete replacement of the detector is therefore planned for the end of 2016 to further guarantee efficient data taking. Following improvements are planned:

Additional detector layers. The current detector layout features three

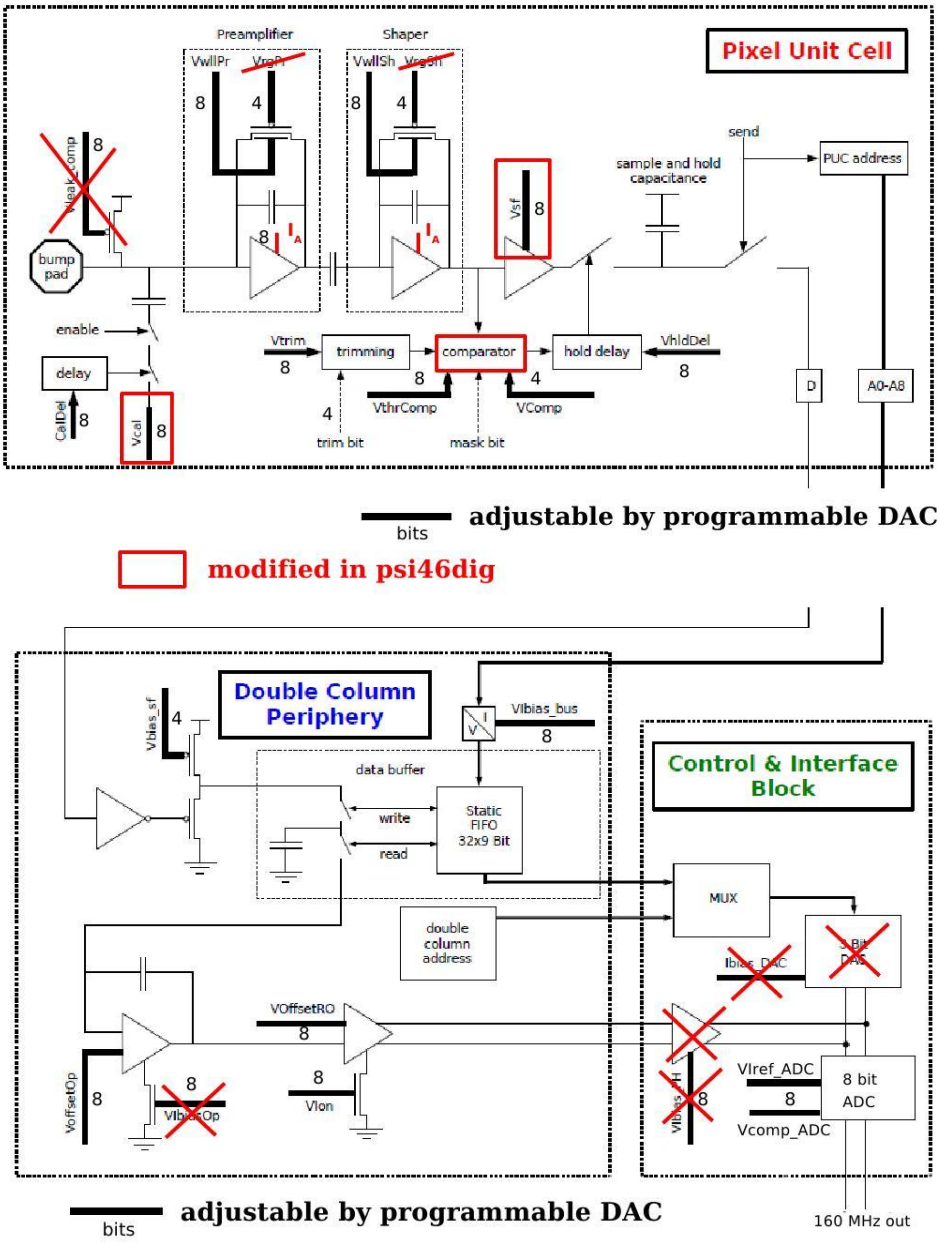

Figure 2.3: Readout chain of the digital ROC. The signal generated by a particle is transmitted to the PUC by a metallic bump pad. Alternatively, a fake signal can be injected; it's strength is regulated by the Vcal DAC. In both cases, the signal passes a preamplifier and a shaper; then, if it is above the threshold set by the trim bits and the VthrComp and Vtrim DACs it is stored in the double column periphery before being converted to a digital signal in the CIB. Also shown are the differences to the old analog ROC [P+ 12].

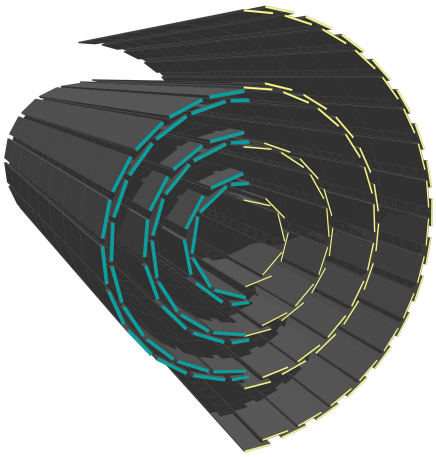

Figure 2.4: The current CMS pixel detector (left) has three layers of modules in the barrel part, while the upgraded one (right) has four. The innermost layer will be moved closer to the beam pipe to improve vertex reconstruction [D+12].

layers in the barrel section and two layers in the end caps. The upgraded detector will have one additional layer. The innermost layer will be moved closer to the beam pipe to allow a more precise vertex reconstruction; see Figure 2.4.

Reduction of material budget. This reduces multiple scattering and energy loss that cannot be measured in the calorimeters.

New readout chip. The new ROC version, called *psi46V2.1respin*, has larger timestamp and data buffers, digital readout, reduced crosstalk and a lower threshold (1800 electrons, reduced from 3500 electrons of the current ROC). Other features of the ROC like amplifier and column drain mechanism are inherited from the analog ROC which is currently used in the detector. The ROC *psi46V2.1respin* will be mounted in layers two to four of the upgraded pixel detector; dedicated ROCs for even higher occupancies are currently being designed for layer one.

2.5 Trimming, or: setting a uniform threshold

As explained in section 2.3, a signal is read out from the PUC only if it exceeds a tunable threshold. The threshold is needed to separate actual signals from the inevitable background noise. It is important for all pixels to have the same threshold, since they should respond in the same way to a given signal. In particular, a single particle can hit a cluster of two or more adjacent pixels, and this can be used to improve the spatial resolution of the detector by computing the centre of the generated charge. It is clear that this is not possible if the outputs of different pixels cannot be compared to each other. The threshold is set individually for each PUC and adjusted by three parameters: *VthrComp*, *Vtrim* and the trim bits. The procedure that sets the threshold of all pixels to a uniform value is called

trimming. It takes as input the target threshold value in *Vcal* units and finds the best values for *VthrComp*, *Vtrim* and the trim bits such that the threshold distribution of all pixels is as narrow as possible and centred at the target value. The algorithm that does this will be described in detail in Chapter 4. Trimming is the main subject of this project, which in particular will focus on how the DAC parameters relevant for the threshold and the trim bits are affected by different working temperatures and accumulation of different amounts of ionizing dose. More details and motivation why this is particularly interesting will be given in the next chapter.

3. Purpose and motivation

This chapter explains the goal of this work. Carrying out the trimming procedure, which will be discussed in detail in Chapter 4, requires to program the DACs of the ROC and to read out the data; these operations are intertwined in the trimming algorithm and how the one is carried out depends on the results of the other in the previous step. In the lab these two operations are both carried out by the digital test board (see section 4.1.3); at the CMS detector they are run by two different systems: front-end controllers (FECs) program the DACs, while front-end drivers (FEDs) read out the data. Since FECs and FEDs do not communicate with each other if not through an external computer, the time needed to trim all the ROCs would be unacceptably long. Trimming has thus to be done in the lab before mounting the modules in the detector. Since the working conditions of the modules like temperature or absorbed radiation dose can and will vary with time, it is important to know how this affects the performance of the module and how possible effects can be reduced.

Temperature dependence of trimming parameters. Before being mounted in the detector, all modules have to be qualified. The qualification procedure consists of a series of tests to verify that the module is working fine with no anomalies. Qualification is done only at 17 °C and −20 °C, but the detector might be working at different temperatures. It is thus important to understand if this affects the threshold of the ROCs and, if so, if and how this can be compensated for by modifying the threshold parameters.

Irradiation effects on trimming parameters. As mentioned in the previous chapter, particles need to deposit some energy in the detector to generate an electrical signal and thus to be detected. Energy is deposited not only in the sensor but also in the ROC; with time, this changes the properties of the transistors and therefore the behaviour of the electronic circuit and of the whole ROC. This happens because traversing particles generate electron-hole pairs also in the oxide layer of the transistors; since the latter is non conducting, the freed electrons cannot recombine with the holes and leave space charges which influence the threshold of the transistor. The amount

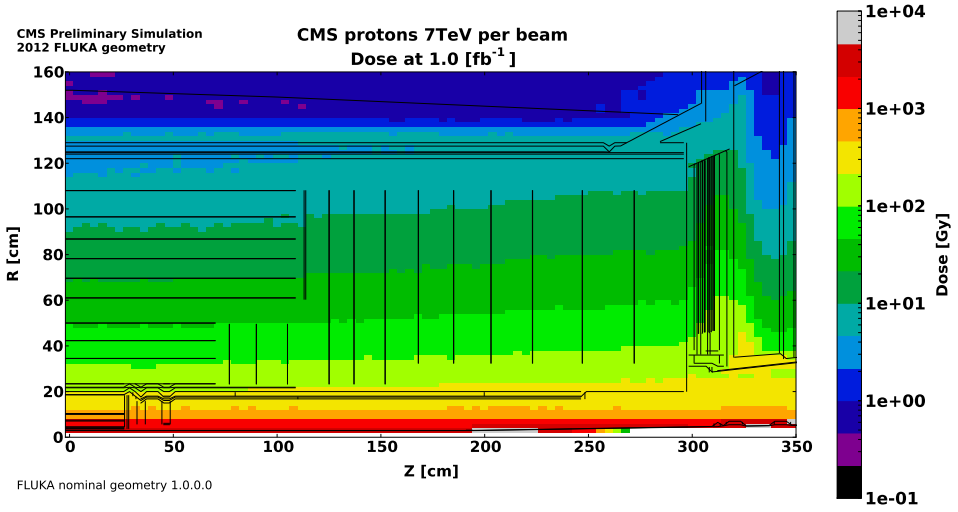

Figure 3.1: FLUKA simulation of dose absorbed by the whole tracker (including the strip detector) with a luminosity of $1.0\,\mathrm{fb}^{-1}$*. With a luminosity of* $500\,\mathrm{fb}^{-1}$*, layer one ROCs are expected to absorb a dose of about* 1.2 MGy *during their lifetime, layer two ROCs about* 0.6 MGy *[Dab15].*

of generated space charge depends on the deposited irradiation dose. The SI unit for absorbed energy dose is the gray [Gy], defined as $1\,\mathrm{Gy} = 1\,\mathrm{J\,kg}^{-1}$. An estimate of the amount of dose absorbed by ROCs in the detector was done with the FLUKA MonteCarlo simulation tool [B+14]. The result for an integrated luminosity of $1.0\,\mathrm{fb}^{-1}$ is shown in Figure 3.1, which shows the whole tracking detector including the strip detector; the pixel detector can be seen in the lower left corner. The new LHC run after LS1 is expected to deliver up to $500\,\mathrm{fb}^{-1}$ of integrated luminosity; for layer one and two this corresponds to a dose of about 1.2 MGy resp. 0.6 MGy. This work aims to understand how the absorbed dose influences the threshold of the ROC and, as in the temperature studies, if an adjustment of the threshold parameters can counteract the effects of irradiation. As mentioned in section 2.4, the currently available chips will be mounted in layers two to four of the CMS pixel detector, while layer one will consist of a different ROC version. The two ROC types will however have many components in common; therefore, studying the behaviour of the *PSI46v2.1respin* ROC at a dose of 1.2 MGy will provide useful information to predict the properties of the layer one ROC.

Shift of the band gap reference voltage

This section describes a known effect of irradiation which has to be taken into account when testing irradiated ROCs. A DAC generates an analog voltage or current based on the digital input value. This output voltage is given by the so called band gap reference voltage (*vbg*) times a certain factor f. A known effect of irradiation is to increase the *vbg* as shown in Figure 3.2.

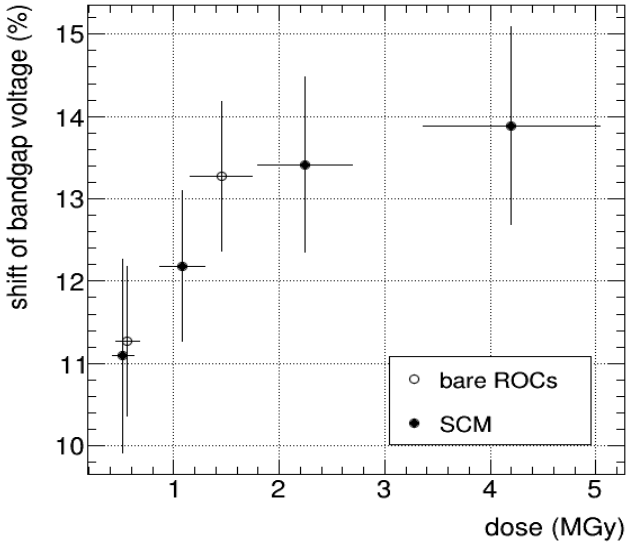

Figure 3.2: Increase of the band gap reference voltage with irradiation dose. According to equation (3.1)*, Vcal 36 after and Vcal 40 before irradiation generate signals of the same strength for samples which absorbed* 0.6 MGy *(vbg shift 11%) or* 1.2 MGy *(vbg shift 12%) [Hos15].*

For the *Vcal* DAC this means that, to obtain the same output voltage (and thus signals of the same strength) as before irradiation, the *Vcal* value has to be lowered according to equation (3.1), where $'$ indicates values after irradiation:

$$\begin{aligned} \text{Output voltage} = Vcal \cdot vbg \cdot f &\stackrel{!}{=} Vcal' \cdot vbg' \cdot f \\ \Rightarrow \quad Vcal' &= Vcal \cdot \frac{vbg}{vbg'}. \end{aligned} \tag{3.1}$$

The doses relevant for this project, 0.6 MGy and 1.2 MGy, cause a *vbg* shift of about 11% resp. 12% (cf. Figure 3.2). Thus a signal generated by *Vcal* 40 before irradiation corresponds in both cases to a signal generated by *Vcal* 36 (rounded to the nearest integer value):

$$Vcal' = 40 \cdot \frac{vbg}{1.11\, vbg} \approx 40 \cdot \frac{vbg}{1.12\, vbg} \simeq 36.$$

It is important to keep this shift in mind when working with irradiated samples.

Before starting with the actual tests, it is advisable to do some reproducibility studies which allow to verify that the trimming routine gives reasonable results, meaning that the values found for *VthrComp*, *Vtrim* and the trim bits are stable if the procedure is repeated at the same conditions. The results of these tests give a measure of the intrinsic variability of the parameters; this later allows to better interpret possible variations of the parameters induced by temperature or irradiation.

4. Setup and procedure

The first part of this chapter describes the testing environment, both hardware and software; the second part presents the testing procedures.

4.1 Hardware

This section presents the hardware components of the testing setup. Most samples are single chip modules (SCM) based on the ROC *psi46V2.1respin*; some tests are performed with bare ROCs without Si sensor. ROCs are controlled and read out by a digital test board (DTB), which is connected to a standard computer running a Linux operating system through a USB cable. During all tests, the samples are placed inside a climatic chamber called cooling box to control humidity and temperature. The bias voltage necessary for depleting the sensor is provided by a Keithley SourceMeter 2400 or 2410 [Kei15].

4.1.1 Samples

The tests are performed with single chip modules (SCMs) like the one shown in Figure 4.1. They consist of a single *psi46V2.1respin* ROC bump bonded to a Si sensor, mounted on a printed circuit board (PCB). The PCB connects the chip to the test board (see below). Tests performed on SCMs provide

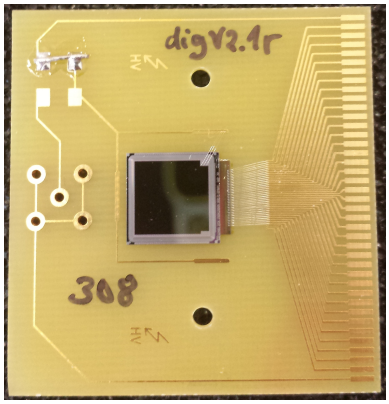

Figure 4.1: Photograph of a single chip module (SCM); it consists of a Si sensor bonded on top of a ROC mounted on a printed circuit board (PCB).

results valid also for whole modules, since they consist of the same subunits, but offer a simplified test setup and readout process. So called bare ROCs, which are used in some of the tests, are SCMs without Si sensor.

Irradiated samples

The samples used for irradiation studies were exposed to a 23 MeV proton beam at Zyklotron AG in Karlsruhe [KIT15, ZAG15]. At this energy, Si has a stopping power of 18.1 MeV $\mathrm{cm}^2\,\mathrm{g}^{-1}$ [NIS15]. To achieve doses of 0.6 MGy and 1.2 MGy (cf. Chapter 3), this requires fluences of 0.2×10^{15} protons/cm^2 and 0.4×10^{15} protons/cm^2 respectively, which can be delivered in a matter of hours by the cyclotron.

Figure 4.2: Cooling box used to control and monitor humidity and temperature of the samples. The hoses in the background provide cooling water for the Peltier elements.

4.1.2 Cooling box

To control the working temperature of the SCMs, during the tests they are placed inside the cooling box shown in Figure 4.2. Any temperature between 17 °C and −20 °C can be obtained through four Peltier elements, which are cooled by a continuous water flow. Before cooling, the test chamber is flushed with dry air to avoid condensation at the lower temperatures. A small flow of dry air is maintained also during tests to keep the humidity low.

4.1.3 Digital test board

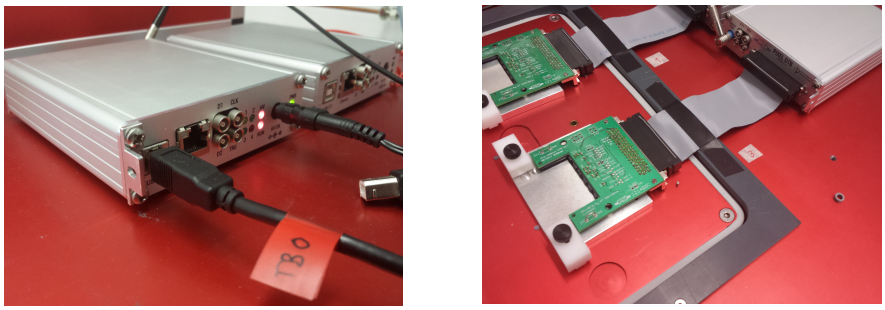

(a) Front view of the DTB.

(b) Rear view of the DTB with single chip adapter.

Figure 4.3

The digital test board (DTB) is the interface used to communicate with the ROC. It controls the settings of the ROC or of a whole module, sends the trigger for calibration signals and reads out the data. On the front panel shown in Figure 4.3(a) there are the power supply cable (on the right) and the USB connection to the computer. Figure 4.3(b) shows the rear view of the DTB, with the bias voltage supply cable and the single chip adapter connected through a flat band cable. The aluminium plate which can be seen beneath the adapter provides thermal contact to the plate cooled by the Peltier elements.

4.2 Software

The computer used for the tests is a standard PC equipped with the operating system Scientific Linux 6 [SL6]. All test routines are implemented in the software *pXar* [pX15], which is written in `C++` and uses the ROOT data analysis framework [BR97]. For some tests also a `python` wrapper calling the *pXar* core functions has been used instead of the graphical user interface of *pXar*.

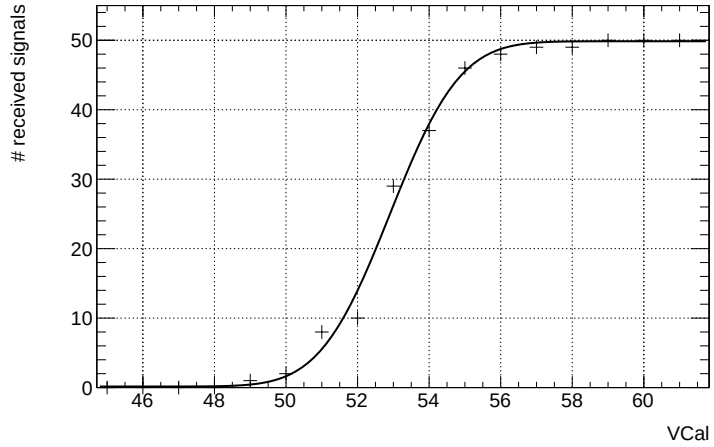

Figure 4.4: Example of an S-curve fitted with an error function.

Two of the test routines should be performed before starting the actual tests to verify basic functionality and to find a working point for some of the essential DAC parameters of the chip:

PreTest checks that the ROC is programmable, i.e. that the DAC parameters can be regulated, sets *Vana* such that the analog current of the chip is 24 mA and finds a good working point in the *CalDel* - *VthrComp* space.

PixelAlive checks that all pixels are working fine by sending a given number of test pulses to each pixel and comparing it to the number of received hits. The procedure is repeated for all pixels of the sample.

The two test procedures most relevant for this project, trimming a ROC to a certain threshold and measuring the resulting threshold distribution, are described in the following two sections.

4.2.1 S-curve measurement

Thresholds are measured with so called S-curves. To measure the *Vcal* threshold, i.e. the *Vcal* value corresponding to the comparator threshold, signals of increasing strength are sent to a pixel with a constant threshold and the response efficiency, i.e. the ratio between received and sent pulses, is observed. If one instead wants to measure which *VthrComp* value corresponds to a certain *Vcal* value, signals of constant strength (i.e. of constant *Vcal* value) are sent to the pixel and *VthrComp* is scanned (remember that *VthrComp* is an inverse DAC, with low values corresponding to high thresholds); again the response efficiency is measured for each *VthrComp* value. Ideally this would give in both cases a step function: all signals above the

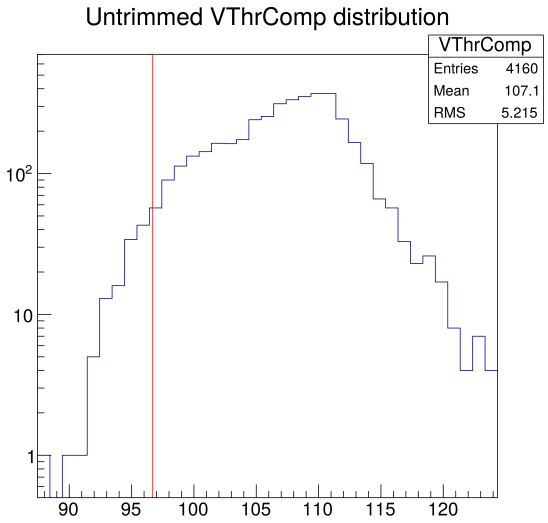

Figure 4.5: VthrComp distribution of a ROC before trimming. The minimal value is chosen above a limit of 2 rms to the left of the mean value to exclude outliers.

threshold are recorded, while those below are lost. In reality noise smears out the threshold, giving an S-shaped curve like the one in Figure 4.4; if the noise follows a Gaussian distribution the curve can be fitted with an error function. The measured threshold value is taken where the curve reaches 50% of the plateau height.

4.2.2 The trimming algorithm

The purpose of the trimming procedure, introduced in Chapter 2, is to unify the threshold of all pixels of a ROC to a certain *Vcal* value (recall that 1 *Vcal* unit corresponds to the charge of about 46 electrons). This means that signals will pass the comparator of the PUC only if they exceed this value and, as described above, it is important for all pixels to have the same threshold. The trimming algorithm implemented in *pXar* takes as only input the target *Vcal* value and comprises four steps:

1. Determine minimal *VthrComp* such that all pixels have a threshold larger than the target value; remember that small *VthrComp* values correspond to a large threshold and that the trim bits can only lower the threshold. *VthrComp* is determined in the following way: *VthrComp* S-curves are measured for each pixel, giving a distribution like the one in Figure 4.5. To avoid picking a possible outlier of the distribution, the minimal *VthrComp*

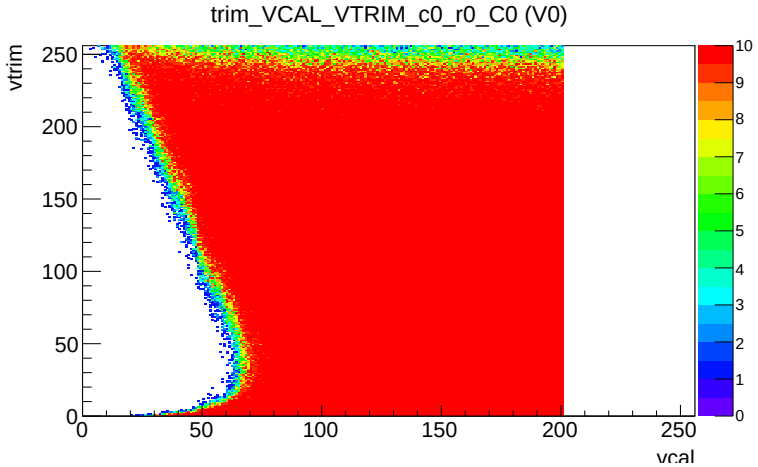

Figure 4.6: Vtrim vs Vcal scan. Chosen is the Vtrim value for which the threshold in a horizontal slice of the distribution is the target Vcal value.

value is taken as the smallest one above a limit defined as

$$\text{minThrLimit} = \text{mean} - n \cdot \text{rms}, \tag{4.1}$$

where the default value for n is 2. Figure 4.5 already shows that this cuts the distribution at a rather arbitrary point and is therefore not the best value, as will be confirmed by reproducibility tests in Chapter 5.

2. Determine pixel with largest *Vcal* threshold. Once the global threshold of the ROC is fixed, the next step is to find how strong the trim bits must be in order to bring all pixels to the desired value, i.e. *Vtrim* must be optimized. To this end the pixel with the largest threshold, i.e. the one furthest from the target value, has to be found. First the *Vcal* threshold distribution is measured. As for *VthrComp*, an upper bound is set to exclude outliers. The limit is taken again n rms away from the mean, this time to the right. Then the measured *Vcal* distribution is scanned to find the pixel that has the largest threshold below the upper limit.

3. Determine *Vtrim* using the pixel with the highest threshold. The trim bit value of the pixel found in the previous step is set to zero; this corresponds to the maximal trimming, i.e. maximal lowering of the threshold. Then the *Vtrim* DAC is scanned: for each *Vtrim* value signals of increasing strength are sent to the pixel and the number of hits is recorded; this is called a *Vtrim* versus *Vcal* DAC-DAC scan and gives a plot like the one in Figure 4.6. The band at the top, which corresponds to very low thresholds, is affected by noise and not considered in the following. Starting just below this region, the plot is scanned to find the *Vtrim* value for which the threshold of the pixel corresponds to the target threshold.

4. Set trim bits. At this point the global threshold of the ROC and the strength of the trim bits are fixed, and the only thing left to do is lower the threshold of each pixel by the right amount by choosing the correct trim bit configuration. This is done with a binary search in four steps: it starts with the trim bits of all pixels set to 7 and a subsequent measurement of the threshold. Depending if the result of the measurement lies above or below the target value, the trim bit of each individual pixel is increased or lowered by 4. At this point another threshold measurement is performed to check if the correction improved the threshold value, i.e. if the corrected threshold is closer to the target than the old one; if not, the correction is reverted. The following step repeats this procedure with a correction of 2, the third and the fourth with a correction of 1. This procedure is able to find the trim bit value for each pixel that brings the threshold as close as possible to the target threshold. At the end, the threshold is measured again for all pixels to validate the procedure. The threshold distributions before and after running the trimming algorithm are shown in Figure 4.7.

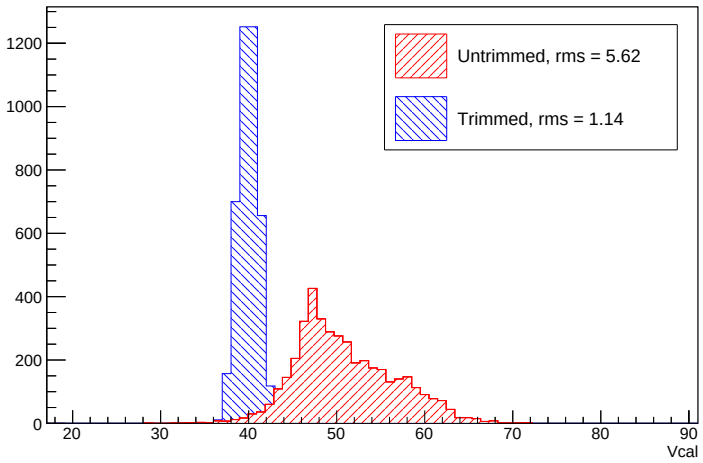

Figure 4.7: Vcal threshold distributions before and after trimming to Vcal 40. The untrimmed distribution is already shifted to the VthrComp value found in the first step of the algorithm. The trimmed distribution is narrow and centred at the target value.

4.3 Testing procedure

Having motivated the project and presented the testing setup and routines, this section describes the testing procedure carried out in order to asses the the questions raised in Chapter 3.

4.3.1 Reproducibility of the threshold parameters

The samples are trimmed ten times to *Vcal* 40 at a temperature of 17 °C to measure the reproducibility of the trimming parameters. This gives a distribution for each parameter, one for each pixel in the case of the trim bits and one for each ROC in the case of *VthrComp* and *Vtrim*. The rms of these distributions are taken as a measure for the reproducibility of *VthrComp* and *Vtrim*. For the trim bits, the rms is averaged over all pixels. As will be shown in detail in the next chapter, two small modifications of the trimming algorithm were made to improve the reproducibility of *VthrComp* and *Vtrim*: how the lower limit for *VthrComp* is chosen in the first step, and the number of triggers for the DAC-DAC scan in the third step.

4.3.2 Temperature dependence of the threshold parameters

This test comprises two parts: first trimming is done at one temperature (17 °C or −20 °C) and with this set of parameters the threshold of the ROC is measured at different temperatures between 17 °C and −20 °C to test a possible temperature dependence of mean and width of the trimmed threshold distribution. Then the ROC is trimmed to the same *Vcal* value at each of these temperatures, and the optimized parameters are compared. This allows to study if the threshold is temperature dependent and to trace the possible dependence of the threshold back to the dependence of a specific parameter.

4.3.3 Effects of irradiation on threshold parameters

As mentioned in section 4.1.1, samples used in irradiation studies received a dose of 0.6 MGy or 1.2 MGy. They were all trimmed before and after being irradiated[1]. After comparing the pre- and post-irradiation trimming results, the *Vcal* threshold is measured with the pre-irradiation parameters to check for effects on the mean and the width of the distribution caused by irradiation. The threshold parameters are then corrected in order to shift the threshold distribution of the ROC back to the original value.

[1] Trimming in this case was done with a `python` wrapper calling the *pXar* core functions. Cross checks showed no difference to results obtained with the *pXar* GUI.

5. Results

This chapter presents the results of the performed tests. First the reproducibility of the threshold parameters is discussed, followed by the studies on the threshold dependence on temperature and irradiation dose.

5.1 Reproducibility of the threshold parameters

Samples used for reproducibility tests are unirradiated single chip modules and bare ROCs. As explained in the previous chapter, they are trimmed ten times each and the rms of the resulting distribution of the parameters *VthrComp*, *Vtrim* and the trim bits is taken as a measure of reproducibility.

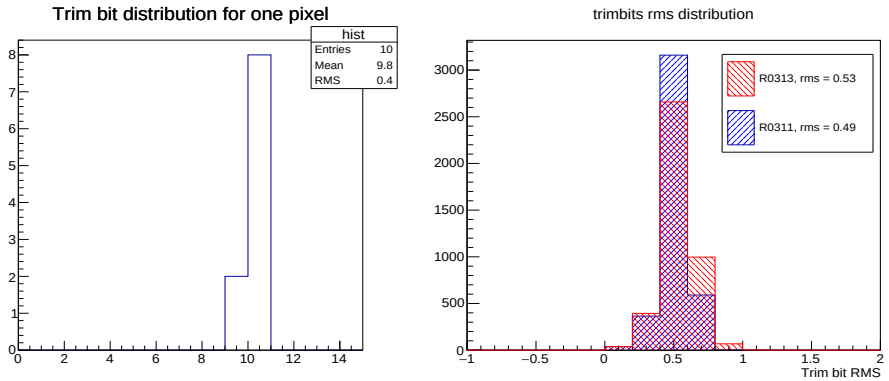

(a) *(b)*

Figure 5.1:

(a) Trim bit distribution of a single pixel after running the trimming ten times. The rms of this distribution taken for all pixels gives the histogram in (b).

(b) Distribution of the rms of the trim bits of all pixels. For both samples the average rms of the trim bits of one pixels is 0.5.

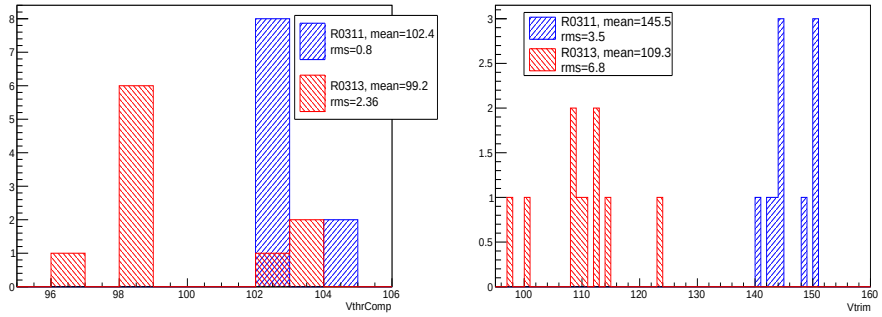

(a) *(b)*

Figure 5.2: VthrComp and Vtrim distributions of both samples found with the default settings of the pXar algorithm.

(a) The VthrComp distributions have an rms of 0.8 (sample R0311) and 2.36 (sample R0313) DAC units.

(b) The Vtrim distributions have an rms of 3.5 (sample R0311) and 6.8 (sample R0313) DAC units.

Trim bit reproducibility

Each pixel of the ROC has a trim bit value optimized to reach the target threshold. For one example pixel the trim bit distribution obtained by repeating the trimming is given in Figure 5.1(a). By filling an histogram with the rms of this distribution of all 4160 pixels of a ROC, the distributions in Figure 5.1(b) are obtained. The mean of these distributions, which is 0.5 for both samples, is taken as a measure of the reproducibility of the trim bits.

Reproducibility of *VthrComp* and *Vtrim*

First reproducibility tests of the DAC parameters *VthrComp* and *Vtrim* produced the results shown in Figure 5.2. *VthrComp* has an rms of 0.8 DAC units for sample R0311 and of 2.36 DAC units for sample R0313, while *Vtrim* has an rms of 3.5 DAC units for sample R0311 and of 6.8 DAC units for sample R0313. In order to improve this rather poor reproducibility of the two DAC parameters, two changes are made to the trimming algorithm: first, the lower limit of *VthrComp*, which is defined in equation (4.1), is lowered to

$$\text{mean of the distribution} - 3 \cdot \text{rms}.$$

This is justified by the plots in Figure 5.3, which show the *VthrComp* distribution measured in the first step of the trimming algorithm for sample R0311 and sample R0008 (the latter is a bare ROC): the new lower limit is

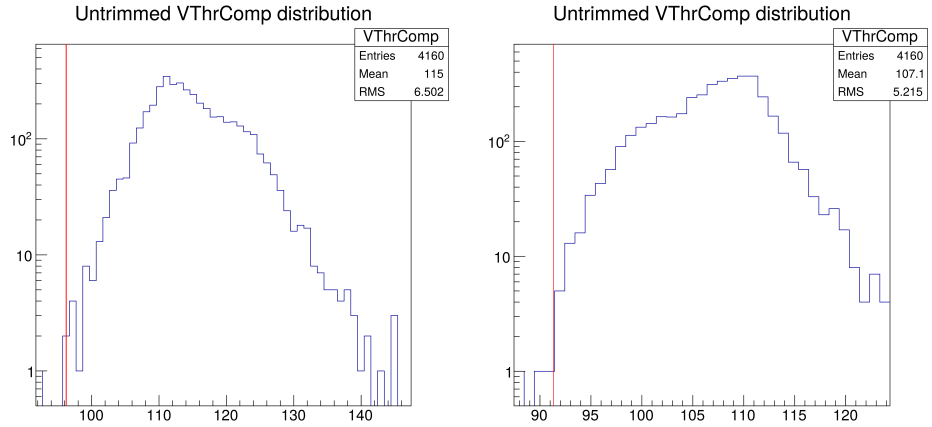

(a) Sample R0311. *(b) Bare ROC R0008.*

Figure 5.3: The lower limit for VthrComp in the first step of the trimming algorithm is lowered from 2 to 3 rms of the distribution to the left of the mean of the distribution. This still efficiently excludes outliers and allows to find values closer to the true minimal VthrComp value of the ROC.

at the left end of the distribution and would still exclude potential outliers. This allows to obtain more reasonable *VthrComp* values, since now the distribution is not cut at an arbitrary value. The second change concerns the determination of *Vtrim*. To narrow the distribution of this parameter, the number of triggers for the DAC-DAC scan in the third step of the algorithm is increased from 10 to 100. By doing so, the transition from where no signals are received (high threshold, weak signals) to the efficient region of the plot is measured with higher resolution (see Figure 5.4), allowing a more precise and stable determination of *Vtrim*. The tradeoff for this is an increase of the duration of the trimming procedure by a factor 5 to about 5 min. The tweaked algorithm run ten times on sample R0311 delivers the DAC values shown in Figure 5.5: the rms of *VthrComp* is reduced from 0.8 to 0.5 DAC units and the rms of *Vtrim* from 3.5 to 2.0 DAC units. From now on this modified algorithm is used.

The results of this section can be summarized as follows: the trim bits are reproducible within an rms of 0.5, *VthrComp* within an rms of 0.5 DAC units and *Vtrim* within an rms of 2.0 DAC units.

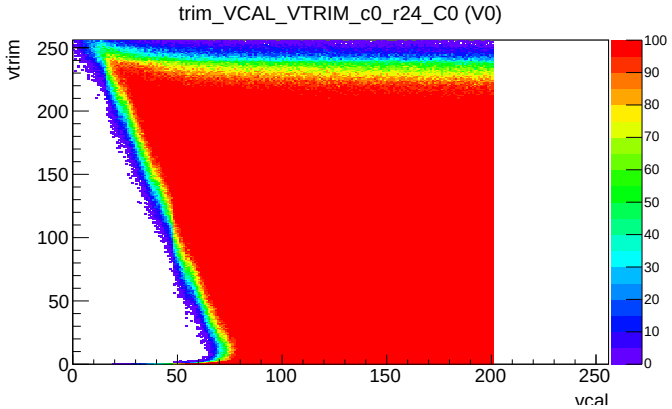

Figure 5.4: The number of triggers in the Vtrim vs Vcal scan was raised from 10 to 100. This increases the resolution of the measured response efficiency and thus stabilizes the obtained Vtrim values.

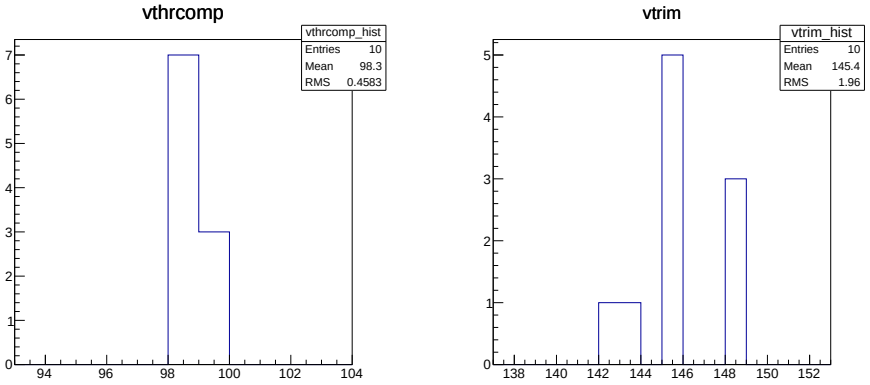

(a) *(b)*

Figure 5.5: Results of the tweaked trimming algorithm run ten times on sample R0311. The rms is reduced from 0.8 to 0.5 DAC units for VthrComp (a) and from 3.5 to 2.0 DAC units for Vtrim (b).

5.2 Temperature dependence of the threshold

This section presents the results of the temperature dependence tests described in section 4.3.2. The two SCMs used for the tests are first both trimmed to *Vcal* 40 at 17 °C and −20 °C; the *Vcal* thresholds are then measured at intermediate temperatures, first with the parameters optimized at 17 °C and then with those optimized at −20 °C. The results are shown in Figure 5.6: for both samples and both trimming temperatures the measured *Vcal* threshold increases linearly with temperature with a slope of 0.2 *Vcal* units/K.

One of the samples is then trimmed at each of the temperatures at which the thresholds were measured to find which parameter is responsible

for the shift of the threshold; *VthrComp* is the only parameter that shows a systematic linear behaviour, while the others change only within their reproducibility as shown in Figure 5.7; this means that for *Vtrim* and the trim bits no temperature dependence is observed. The linear behaviour of *VthrComp* found when trimming the ROC at different temperatures is shown in Figure 5.8 by the green crosses.

As a next step, these values of *VthrComp* are used to correct the shift of the threshold distribution with temperature. As it turns out, to make the threshold temperature independent for a set of trimmed parameters it is not enough to use these exact values, but some corrections of ± 1 or 2 DAC units are necessary (notice that this is within the reproducibility of *VthrComp*). The corrected values, found iteratively, are marked by the triangles in Figure 5.8 and allow to obtain the temperature independent thresholds shown in Figure 5.9. All other parameters, trimmed at 17 °C resp. −20 °C, are unchanged. The effect of this correction of *VthrComp* is a slight broadening of the measured *Vcal* threshold distribution from about 1.1 DAC units, corresponding to 51 electrons, to about 1.4 DAC units, corresponding to 64 electrons, as shown in Figure 5.10.

Based on the results of the first sample, also the threshold of the second is corrected by iteratively finding the *VthrComp* value that compensates the shift due to temperature change. The results, very similar to those of the first sample, are shown in Figure 5.11. The iteratively found values of *VthrComp* that keep the threshold constant can be parametrized with a linear function with a slope of 0.2 DAC units/K. No other parameters are changed from the initial trimmings at 17 °C and −20 °C. The correction of *VthrComp* broadens the threshold distribution by the same amount as for the first sample, from about 1.1 DAC units (51 electrons) to about 1.4 DAC units (64 electrons).

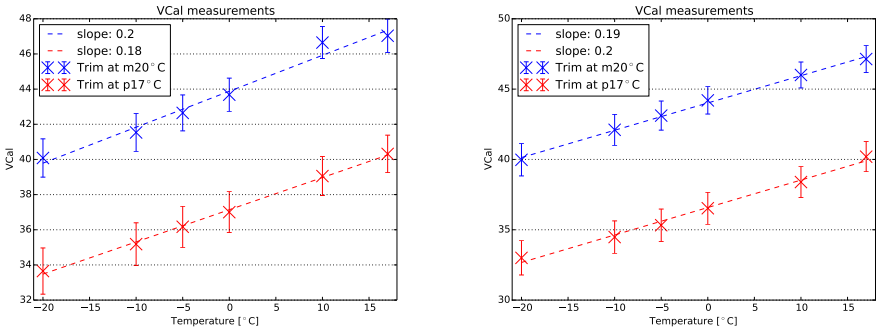

(a) Sample R0311. *(b) Sample R0321.*

Figure 5.6: Both ROCs are trimmed to Vcal 40 at 17 °C *(red) and* −20 °C *(blue). With the parameters found at these trimmings fixed, the measured Vcal threshold increases with temperature with a slope of 0.2 Vcal units/*K.

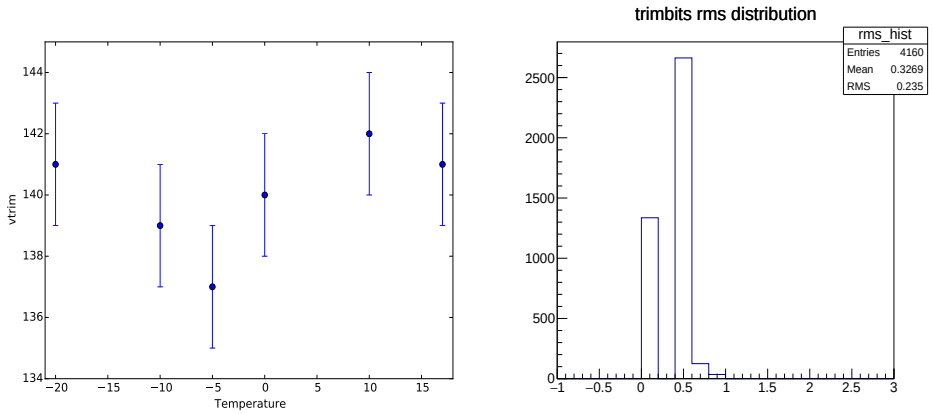

(a) *(b)*

Figure 5.7: Vtrim values (a) and distribution of the rms of the trim bits of each pixel (b) after trimming sample R0311 at several temperatures. Vtrim has an rms of 1.8, while the mean of the trim bit rms distribution is less than 0.5. Vtrim and trim bits thus change only within their reproducibility without any temperature dependence.

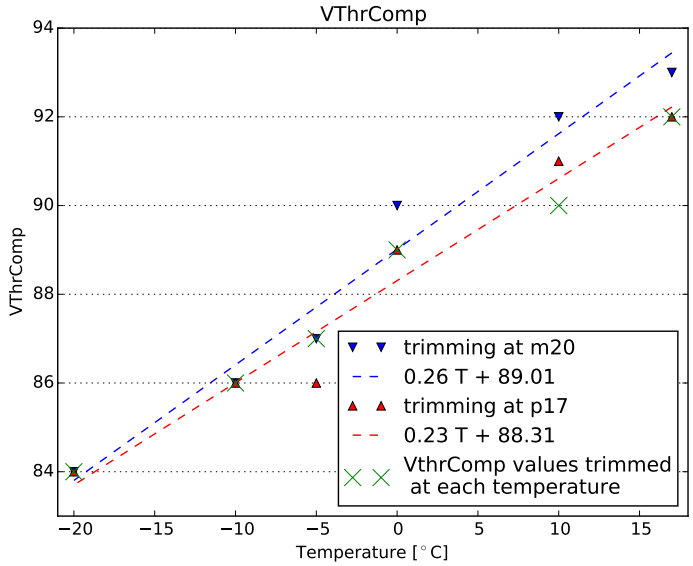

Figure 5.8: Linear dependence of VthrComp on temperature for sample R0311. The crosses mark the values found by trimming at the respective temperature; the triangles mark the values found iteratively to keep the threshold as constant as possible while leaving the other parameters unchanged. The up pointing ones correct the threshold for the parameters found by trimming at 17 °C, the down pointing ones for the parameters from trimming at −20 °C. Linear fits provide very similar slopes for the two parameter sets and can be used as parametrization for VthrComp at different temperatures.

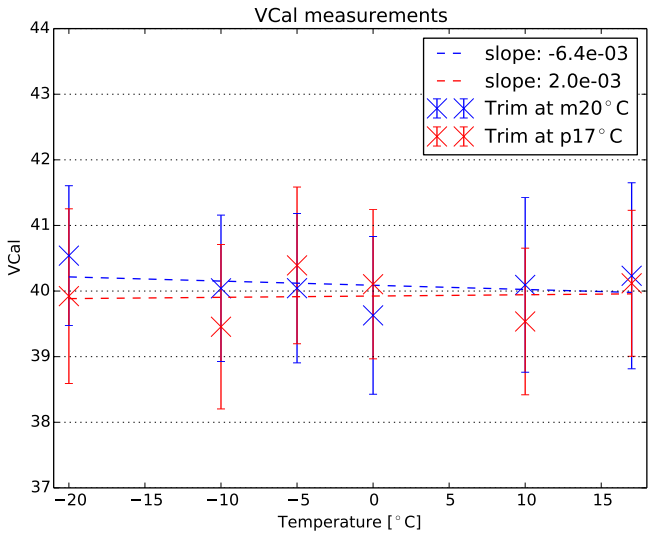

Figure 5.9: Vcal threshold distributions of sample R0311 (cross: mean, error bars: rms) measured at several temperatures with the corrected VthrComp values marked by the triangles in Figure 5.8 and the other parameters unchanged. By correcting VthrComp following the parametrization of Fig. 5.8 it is possible to obtain a temperature independent threshold.

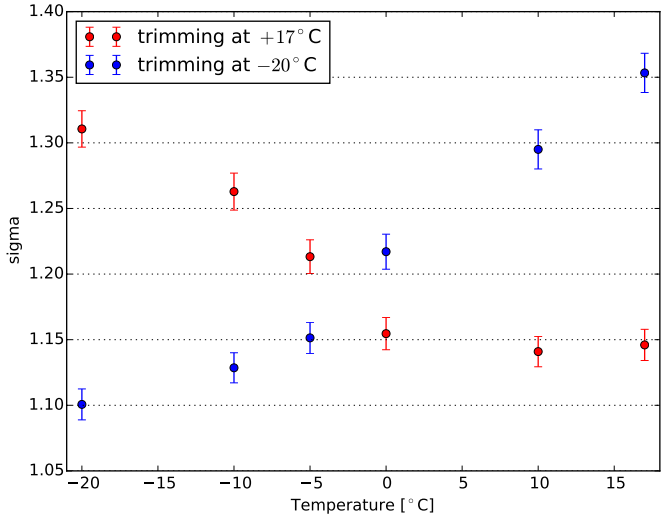

Figure 5.10: Width of the temperature independent Vcal threshold distribution (fitted with a Gaussian) of sample R0311 after correcting VthrComp. The change of VthrComp induces a broadening of the distribution from about 1.1 DAC units to about 1.4 DAC units, corresponding to 51 electrons and 64 electrons respectively.

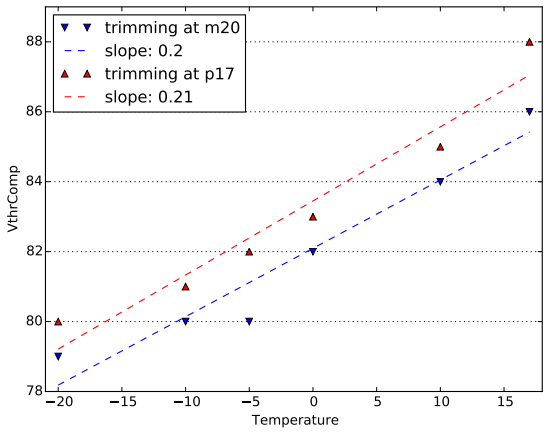

(a) VthrComp values that keep the Vcal threshold of sample R0321 constant, cf. Fig. 5.8.

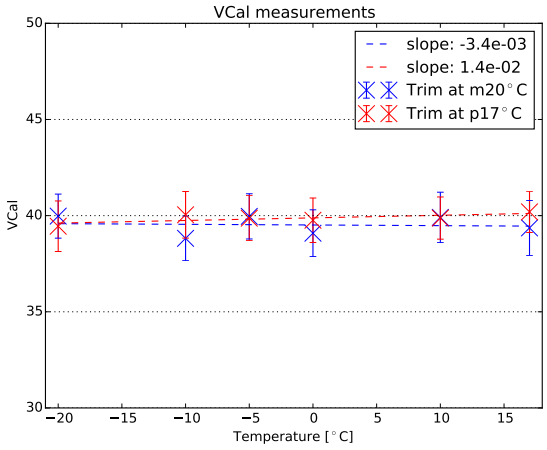

(b) Vcal thresholds measured with VthrComp values from (a), cf. Fig. 5.9.

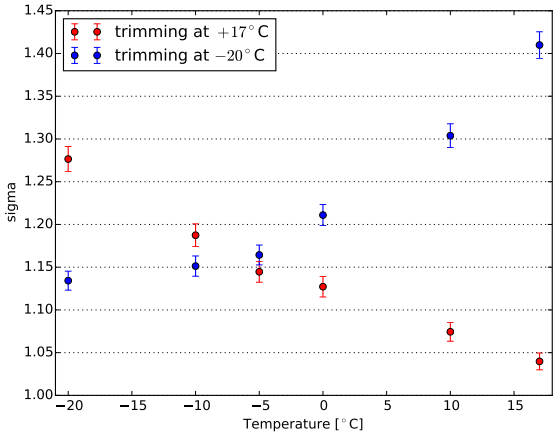

(c) Broadening of the Vcal threshold due to changing VthrComp, cf. Fig. 5.10.

Figure 5.11: Sample R0321 shows a behaviour analogous to sample R0311: the VthrComp setting found to obtain a temperature independent threshold changes linearly with a slope of 0.2 DAC units/K (a). Vcal thresholds measured with the corrected VthrComp values (b). As a trade off, the threshold distribution broadens from 1.1 DAC units (51 electrons) to 1.4 DAC units (64 electrons) (c).

5.3 Dose dependence of the threshold

This section presents the results of the irradiation studies described in section 4.3.3. From a total of six tested samples, two (labelled R0302 and R0303) received a radiation dose of 0.6 MGy, and four (R0304, R0305, R0306 and R0309) a dose of 1.2 MGy. All samples have been trimmed both before and after being irradiated, where the trimming was executed before the beginning of this project. The comparison of the trim bit distributions optimized before and after irradiation is shown in Figure 5.12. A clear difference between the pre- and post-irradiation distributions can be seen, although it is not perfectly consistent among the samples. To better quantify this, the difference of post- and pre-irradiation trim bit values is taken for each pixel and filled into an histogram; mean and width of the resulting distributions are shown for all samples in Figure 5.13. In this plot, a narrow distribution centred at 0 would indicate that there has been no change of the trim bits; instead, the distributions are for most samples shifted from 0 to positive values, indicating an increase of the trim bit values of the pixels and have a width of 1-2 trim bits. Sample R0304 does not follow this trend and is the only outlier with a negative shift of -2 trim bit units.

In the next step the *Vcal* threshold distribution is measured with the threshold parameters optimized before irradiation. The rms of the distribution is broader by a factor 2-3 and the mean is shifted to lower *Vcal* values. To compensate the shift, *VthrComp* is corrected iteratively, in a way similar as for the temperature studies in section 5.2. Figure 5.14 shows three *Vcal* threshold distributions for sample R0309: measured before irradiation with optimized parameters, with the same parameters after irradiation and with corrected *VthrComp*. The thresholds measured with the pre-irradiation parameters after irradiation are summarized for all samples in Figure 5.15. The threshold does not shift monotonously with irradiation dose, but decreases by about 15 *Vcal* units for the 0.6 MGy samples and by only 10 *Vcal* units for the 1.2 MGy samples. To counteract the shift of the *Vcal* threshold, *VthrComp* is corrected iteratively to get the threshold back to the original physical value, which, due to the band gap reference voltage shift, after irradiation corresponds to *Vcal* 36 (cf. end of Chapter 3). The obtained *VthrComp* values are shown in Figure 5.16. The magnitude of the correction reflects the threshold shift: the 0.6 MGy samples require a correction of 17 ± 2 *VthrComp* units, the 1.2 MGy samples of 10 ± 3 *VthrComp* units. By doing so, the mean of the distribution of all samples can be shifted to a value corresponding to the same threshold as before irradiation as shown in Figure 5.17. As already seen during temperature dependence studies, the correction of *VthrComp* comes with an increase in the width of the threshold distribution, here by 0.5-1 *Vcal* units, see Figure 5.18. For comparison, also shown are the widths of the distributions obtained by re-optimizing the trim bits with a new trimming after irradiation. These have a width of

about 1 *Vcal* unit, but cannot be obtained at CMS, since trimming is not possible there.

As a last step, it was analysed if optimizing *Vtrim* after the correction of *VthrComp* could allow to narrow the *Vcal* threshold distribution. The results are shown in Figure 5.19: by changing *Vtrim*, the mean of the distribution gets shifted as expected but the rms is unaffected. This means that changing *Vtrim* provides no useful way to reduce the width of the threshold distribution.

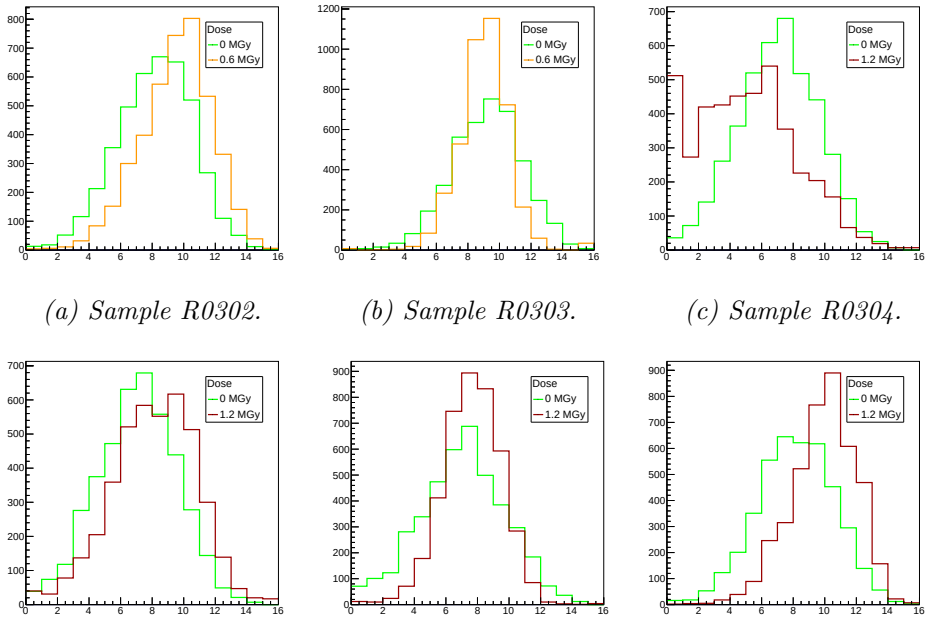

(a) Sample R0302. *(b) Sample R0303.* *(c) Sample R0304.*

(d) Sample R0305. *(e) Sample R0306.* *(f) Sample R0309.*

Figure 5.12: Trim bit distributions of all samples obtained by trimming before (green) and after (orange/red) they were irradiated.

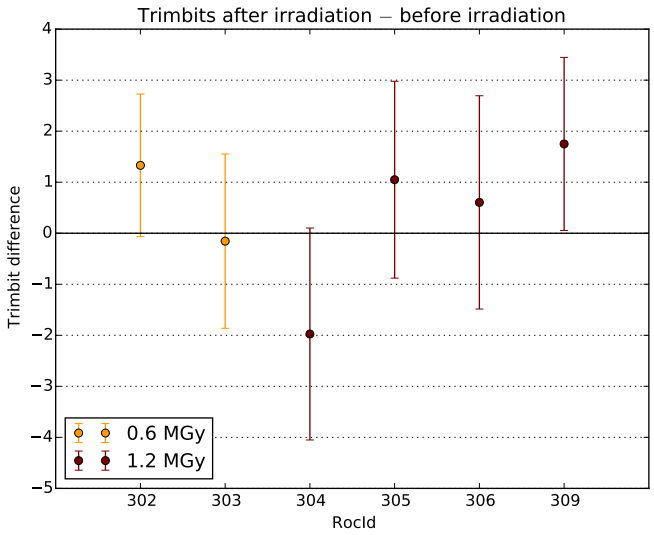

Figure 5.13: Mean and rms of the trim bit difference of each pixel for the different samples. The tendency is a shift to higher trim bit values, with the exception of sample R0304.

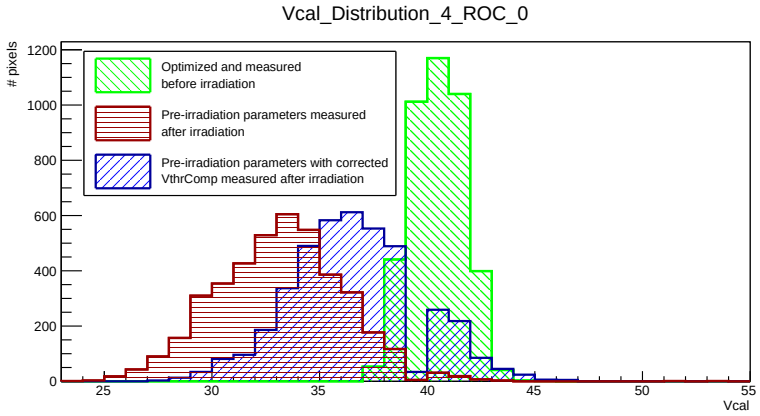

Figure 5.14: Vcal threshold distributions of sample R0309 optimized and measured before irradiation (green), measured after irradiation with the same parameters (red) and after correcting VthrComp to shift the mean of the distribution back to the original threshold (blue); Vcal 36 after and Vcal 40 before irradiation correspond to the same physical threshold because of the band gap reference voltage shift. After irradiation the distribution is shifted and the rms is bigger by a factor 2-3.

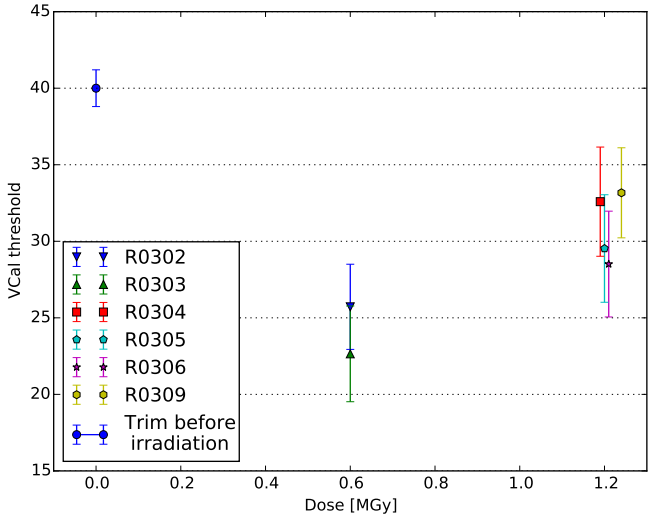

Figure 5.15: Before irradiation all ROCs are trimmed to Vcal 40; using the same trimming parameters after irradiation, the Vcal threshold decreases and its rms increases by a factor 2-3.

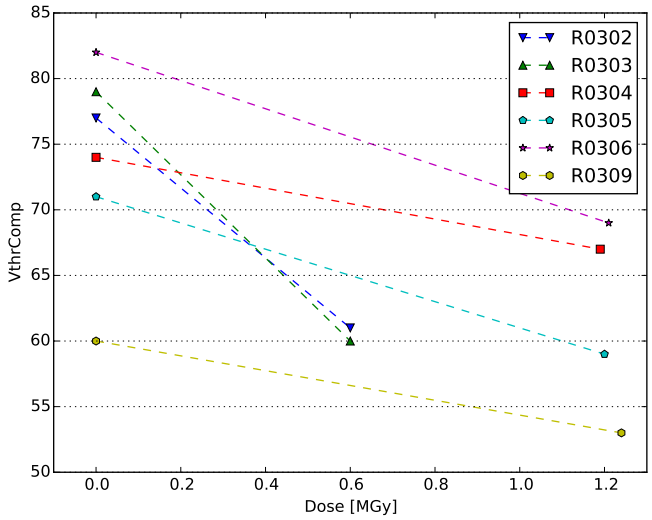

Figure 5.16: VthrComp values obtained by trimming before irradiation and corrected VthrComp values after irradiation (found iteratively). For the 0.6 MGy *samples the correction is of* 17 ± 2 *VthrComp units, for the* 1.2 MGy *samples of* 10 ± 3 *VthrComp units.*

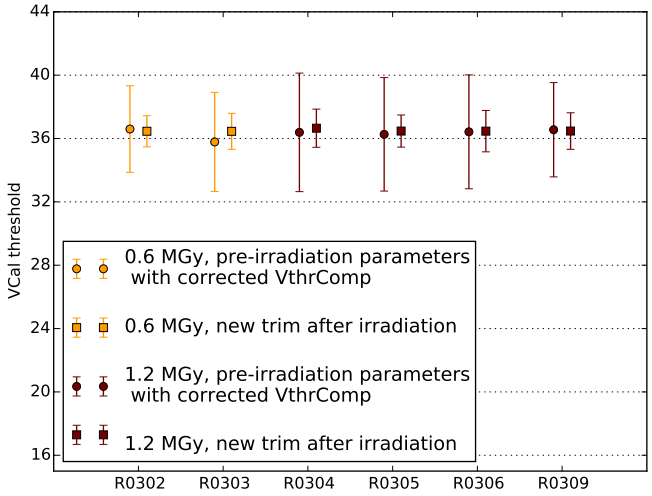

Figure 5.17: Vcal thresholds of the irradiated samples with pre-irradiation trimming parameters and corrected VthrComp (circles) and with all parameters optimized after irradiation (squares). All thresholds are near the target value of Vcal 36; the corrected distributions have a width of about 3.5 Vcal units and the optimized ones of about 1 Vcal unit as shown in Figure 5.18.

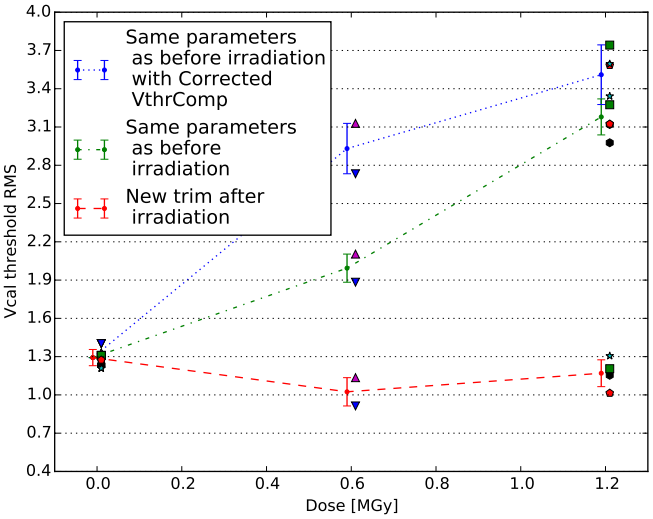

Figure 5.18: Widths of the Vcal threshold distributions measured with the pre-irradiation trimming parameters (green, dot-dashed), with corrected VthrComp (blue, dotted) and when trimmed again after irradiation (red, dashed). The narrowest distributions cannot be achieved at CMS since trimming is not possible in the detector, and the pre-irradiation settings with unchanged VthrComp provide a shifted threshold as shown before. Correcting VthrComp causes a broadening of the distribution by about 0.5-1 Vcal units.

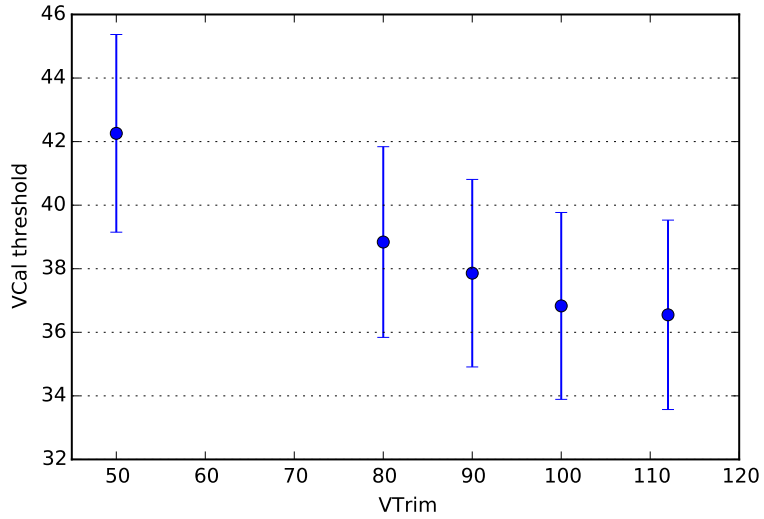

(a)

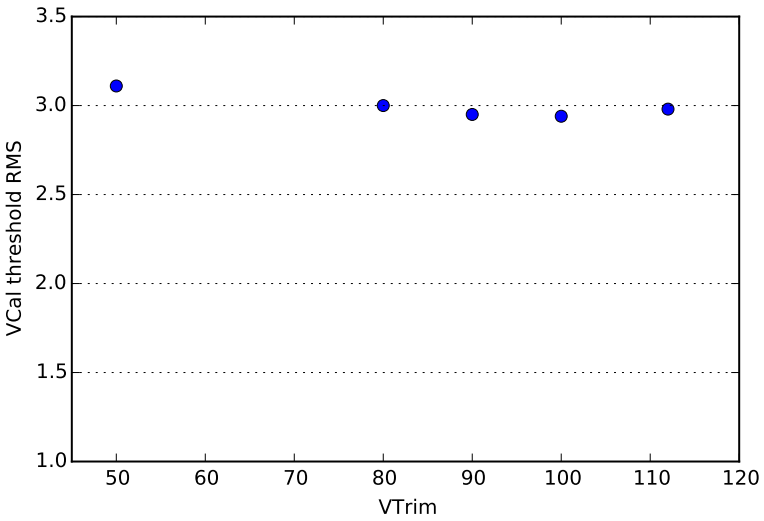

(b)

Figure 5.19: Changing Vtrim causes a shift of the mean of the Vcal threshold distribution (a), but does not change the rms (b).

6. Conclusion and outlook

The aim of this work was to study the effects of temperature changes and irradiation on the threshold of the digital readout chip for the Phase I Upgrade of the CMS pixel detector. The first tests studied the reproducibility of the parameters that are used to set the threshold of the individual pixels of a readout chip; knowing the reproducibility of the different parameters allows to interpret possible changes with temperature or irradiation dose. The tests showed that the trim bits are reproducible within 0.5 trim bit units, *VthrComp* within 0.5 DAC units and *Vtrim* within 2.0 DAC units.

Temperature dependence tests showed that the threshold changes linearly with temperature with a slope of about 0.2 *Vcal* units/K. This shift can be compensated for by adjusting the *VthrComp* DAC by about 0.2 *Vcal* units/K while leaving the other parameters unchanged. The consequence of this correction is a moderate broadening of the rms of the *Vcal* threshold distribution from about 1.1 DAC units to 1.4 DAC units, corresponding to 51 electrons and 64 electrons, respectively.

After irradiation the threshold of the ROC is decreased by a dose dependent amount. The shift is not linear with absorbed dose: the threshold decreases by about 15 *Vcal* units for the 0.6 MGy samples and by only 10 *Vcal* units for the 1.2 MGy samples. Additionally, the rms of the threshold distribution gets wider by a factor 2-3. As for the temperature effect, the shift was thwarted by correcting *VthrComp*, which increased the width of the threshold distribution by 0.5-1 *Vcal* units. The rms of the threshold distributions of all irradiated samples was, after the correction of *VthrComp*, about 3.5 *Vcal* units; this is a rather large value compared to the width of about 1 *Vcal* unit of a freshly trimmed distribution. An attempt to make the distribution more narrow was done by trying to change the *Vtrim* DAC, but this did not solve the problem. The cause for this significant broadening lies in the change of the optimal trim bit configuration observed after irradiation: with the exception of one sample, the trim bits of all ROCs were shifted to higher values. Currently there is no known way to obtain a narrow threshold distribution after the ROC was irradiated without a new trimming. It is advisable to further investigate if this can be achieved. If not, the broad threshold distribution has to be taken into account when operating the detector. A more ambitious solution would be

to find a method to trim the ROCs once they have been mounted in the detector; in this way the thresholds of all ROCs could be periodically re-optimized after a significant amount of dose has been absorbed, delivering a narrow distribution. But, as mentioned above, this appears to be a very complicated and time consuming procedure and is currently not foreseen.

Bibliography

[ATL12] ATLAS Collaboration, *Observation of a new particle in the search for the Standard Model Higgs boson with the ATLAS detector at the LHC*, arXiv:1207.7214 (2012).

[BR97] R. Brun and F. Rademakers. ROOT - An Object Oriented Data Analysis Framework, [Online] July 1, 2015, `https://root.cern.ch`.

[B+14] T.T. Böhlen et al., *The FLUKA Code: Developments and Challenges for High Energy and Medical Applications*, Nuclear Data Sheets 120, 211-214 (2014).

[C+09] G.B. Cerati et al. *Radiation Tolerance of the CMS Forward Pixel Detector.* Nucl. Inst. & Meth. in Phys. Res. A, 600(2):408 – 416 (2009).

[CER15a] CERN, *The LHCb Detector*, [Online] July 1, 2015, `http://lhcb-public.web.cern.ch/lhcb-public/en/detector/Detector-en.html`.

[CER15b] CERN Press release, [Online] June 3, 2015, *LHC experiments are back in business at a new record energy*, `http://press.web.cern.ch/press-releases/2015/06/lhc-experiments-are-back-business-new-record-energy`.

[CMS12] CMS Collaboration, *Observation of a new boson at a mass of 125 GeV with the CMS experiment at the LHC*, arXiv:1207.7235 (2012).

[CMS15] CMS, *Detector overview*, [Online] July 1, 2015, `http://cms.web.cern.ch/news/detector-overview`.

[D+12] A. Dominguez et al., *CMS Technical Design Report for the Pixel Detector Upgrade*, [Online] July 1, 2015, `http://cds.cern.ch/record/1481838/files/CMS-TDR-011.pdf` (2012).

[Dab15] A. Dabrowski, *BRIL Radiation Simulation*, [Online] July 6, 2015, `https://twiki.cern.ch/twiki/bin/view/CMSPublic/BRILRadiationSimulation`.

[DES15] DESY, *DESY CMS group*, [Online] July 1, 2015, http://cms.desy.de.

[Hos15] J.H. Hoß, PhD thesis in preparation.

[Kei15] Keithley 2400 High-Voltage SourceMeter, [Online] July 1, 2015 http://www.keithley.com/products/semiconductor/sourcemeasureunits/series2400sourcemeter/dcac/currentvoltage/2400smu.

[KIT15] Karlsruhe Institute of Technology, *The Cyclotron and the Irradiation Setup*, [Online] July 7, 2015, https://www.ekp.kit.edu/english/264.php.

[LHC12] LHC Performance and Statistics, [Online] July 1, 2015, https://acc-stats.web.cern.ch/acc-stats/#lhc/.

[NIS15] National Institute of Standards and Technology, *Stopping-Power and Range Tables for Protons*, [Online] July 6, 2015, http://physics.nist.gov/PhysRefData/Star/Text/PSTAR.html.

[P+12] D. Pitzl et al.: *Digital ROC beam test results* [Online], [Online] July 1, 2015, http://cms.desy.de/sites/site_cms/content/e53612/e155175/e155178/e157748/e169877/240812-dp.pdf (2012).

[pX15] Pixel Xpert analysis & readout, [Online] July 1, 2015, https://github.com/psi46/pxar.

[R+06] L. Rossi et al. *Pixel Detectors: From Fundamentals to Applications.* Springer-Verlag, Berlin Heidelberg (2006).

[Rut11] E. Rutherford, *The Scattering of α and β rays by Matter and the Structure of the Atom*, Philosophical Magazine. Series 6, vol. 21. (1911).

[SL6] Fermilab, *Scientific Linux 6*, [Online] July 1, 2015, https://www.scientificlinux.org/.

[ZAG15] ZAG Zyklotron AG *Homepage*, [Online] July 6, 2015, http://www.zyklotron-ag.de/en/.